International Journal of Nanomedicine

Dovepress
Taylor & Francis Group

Open Access Full Text Article

ORIGINAL RESEARCH

NIR-Triggered siRNA Release and Lysosomal Escape for Synergistic Photothermal Tumor Therapy

Myagmarsuren Baldan[1–3], Shuang Zhang[1–3], Qi Sun[1–3], Yan Su[3,4], Dong Mei[3,5], Ran Sun[1–3], Ao Zheng[1–3], Danni Liu[1–3], Jie Zhang[1–3], Ran Huo[1–3], Yang Tian[1–3], Le Han[1–3], Shibo Wang[1–3], Yaoqi Wang[1–3], Chunying Cui[1–3]

[1]School of Pharmaceutical Sciences, Capital Medical University, Beijing, People's Republic of China; [2]Beijing Area Major Laboratory of Peptide and Small Molecular Drugs, Beijing Laboratory of Biomedical Materials, Engineering Research Center of Endogenous Prophylactic of Ministry of Education of China, Beijing, People's Republic of China; [3]Laboratory for Clinical Medicine, Capital Medical University, Beijing, People's Republic of China; [4]Medical Oncology Department, Pediatric Oncology Center, Beijing Children's Hospital, Capital Medical University, National Center for Children's Health, Beijing, People's Republic of China; [5]Department of Pharmacy, Beijing Children's Hospital, Capital Medical University, National Center for Children's Health, Beijing, People's Republic of China

Correspondence: Chunying Cui; Yaoqi Wang, Department of Pharmaceutics, School of Pharmaceutical Sciences, Capital Medical University, No. 10 Youanmenwai Street, Fengtai, Beijing, 100069, People's Republic of China, Tel +86-10-8391-1668; +86-10-8391-1673, Email ccy@ccmu.edu.cn; wangyaoqi@ccmu.edu.cn

Background: Resistance to traditional treatments has spurred research into innovative therapeutic approaches for tumors. Among these innovative treatments, photothermal therapy (PTT) has gained increasing attention for its use of photothermal agents (PTAs) to convert light into heat for localized tumor ablation. However, PTT faces limitations due to heat shock protein 70 (HSP70)-mediated resistance in tumor cells. Combining PTT via indocyanine green (ICG) with siRNA HSP70 could reduce the thermal resistance of the tumor, thereby enhancing treatment efficacy. Albumin-based nanoparticles (NPs) can effectively deliver ICG and siRNA into tumor cells. When exposed to near-infrared (NIR) light, these nanoparticles trigger lysosomal escape and release, further enhancing gene silencing activity.

Methods: This study aimed to develop a biocompatible delivery system, HSA@ICG/siRNA NPs, for photothermal-enhanced tumor therapy. The nanoparticles were characterized for size, charge, surface functionalization, and photoconversion properties. In vitro antitumor efficacy was evaluated using MTT assay, calcein AM/PI staining, RT-PCR, and Western blot in 4T1 tumor cells. In vivo, we assessed photothermal effects, biodistribution, tumor inhibition, and biosafety following irradiation.

Results: Characterization confirmed the successful synthesis of uniform, stable HSA@ICG/siRNA NPs with effective photothermal conversion properties. Cellular uptake studies revealed high siRNA internalization, with laser-induced lysosomal escape enhancing cytoplasmic delivery. In vitro, gene silencing reduced mRNA and protein levels by 82.8% and 65%, respectively. In vivo, local tumor temperature increased to 42°C within 3 minutes, indicating a mild but effective photothermal effect. Tumor inhibition rates were 50.00% ± 9.16% for HSA@ICG and 71.26% ± 7.92% for HSA@ICG/siRNA, demonstrating enhanced tumor suppression. The treatment achieved sustained tumor targeting with minimal off-target toxicity.

Conclusion: As a dual-function photothermal therapy agent, HSA@ICG/siRNA NPs combine targeted gene silencing with photothermal effects, demonstrating significant therapeutic promise. This integrated approach addresses tumor resistance, offering a potential advancement in cancer treatment strategies.

Keywords: photothermal therapy, human serum albumin, HSP70 siRNA, lysosome escape, gene silencing

Introduction

Cancers are among the leading threats to human health due to their complex pathogenesis and rising incidence.[1,2] Traditional treatments include surgery, chemotherapy, and radiation therapy.[3] These treatments are mostly limited or accompanied by side effects, such as high toxicity, non-target distribution, short half-life, and multi-drug resistance.[4,5] Given these limitations, several emerging therapies such as photothermal therapy (PTT), photodynamic therapy (PDT), chemodynamic therapy (CDT), and immunotherapy have gained attention as potential alternatives.[6] Among these, PTT has garnered significant interest due to its minimally invasive nature, spatial precision, and ability to convert light into localized heat for tumor

Received: 11 December 2024
Accepted: 26 March 2025
Published: 16 April 2025

ablation. This technique offers the advantage of precise, targeted treatment, addressing some limitations associated with traditional cancer therapies.[5,7,8]

A crucial element for effective PTT is a high-quality photothermal agent. ICG, a near-infrared fluorescent dye with better in vivo clearance and low toxicity, holds FDA approval for in vivo applications.[9–11] ICG exhibits absorption and fluorescence maxima in the NIR region, specifically at approximately 780 nm and 820 nm, which are within the biological window for optimal tissue penetration.[12,13] Under 808 nm laser irradiation, ICG can efficiently convert absorbed near-infrared (NIR) laser energy into heat for photothermal therapy.[14] High-power lasers used in PTT can pose a risk by potentially damaging surrounding normal tissues if the local temperature exceeds 46°C to fully ablate tumors.[15]

Therefore, developing NIR-triggered mild PTT is essential for advancing optical cancer treatments, employing low operating temperatures. Mild photothermal heating has been shown to improve the cellular uptake of therapeutic agents and facilitate drug release from nanocarriers within cells, thereby enhancing the anticancer effects in a synergistic manner.[16–18] Upon light irradiation, the activated photosensitizers generate reactive oxygen species (ROS), which disrupt liposomal and lysosomal membranes, thereby releasing the encapsulated drugs into the cytosol.[19–21]

However, using lower temperatures like 40–45°C in modern PTT approaches presents a new challenge: the production of heat shock proteins (HSPs) that could counteract the therapy's damage by enhancing heat tolerance rapidly.[22–25] Among the HSPs, Heat Shock Protein 70 (HSP70) contributes to several oncogenic processes, including anti-apoptotic responses, suppression of antitumor immune responses, promotion of tumor growth, and facilitation of cell migration.[26–30] Previous studies have shown that the overexpression of HSP70 in tumor cells can lead to resistance against various cancer therapies, including PTT.[24,31] Consequently, targeting and inhibiting HSP70 shows promise as a potential mild photothermal therapy, which can solve the problem of high temperature during PTT and achieve excellent therapeutic effect.[32,33] By down-regulation HSP70 expression, the heat resistance of tumor cells can be mitigated, potentially sensitizing them to PTT-induced thermal damage.[34] The utilization of HSP70 siRNA in combination with PTT can be a promising approach to combat the overexpression of HSP70 and enhance the effectiveness of cancer treatment.[34–38]

However, effective delivery of siRNA to target cells is often hindered by challenges such as degradation and limited uptake.[39] Nano-drug delivery carriers have become indispensable in overcoming these obstacles and enhancing the therapeutic efficacy of exogenous siRNA.[40,41] Human Serum Albumin (HSA) is a promising candidate for drug delivery applications due to its inherent natural properties, including biocompatibility, biodegradability, low immunogenicity, and non-toxicity.[42–44] Furthermore, the rapid multiplication of tumor cells requires a large amount of nutrients, and albumin can provide just the right amount of amino acids and energy, making it easy for tumor cells to take up albumin.[45]

The design of HSA@ICG/siRNA nanoparticles leverages the unique structural properties of HSA, enabling efficient loading of both ICG and siRNA through hydrophobic and electrostatic interactions. The structural domain of HSA is a hydrophobic positively charged pocket structure that can form complexes with insoluble or exogenous substances.[46,47] HSA can non-covalently bind ICG into the hydrophobic domain via hydrophobic binding, based on their structure comprising anionic, lipophilic, and aromatic characteristics[12,18,48,49] siRNA can be encapsulated in HSA through desolvation-crosslinking method (Figure 1A).[39,50,51] Our previous studies successfully encapsulated siRNA within BSA nanoparticles using the same method and subsequently optimized the preparation.[39,50]

Synergistic enhancement of PTT including ICG and siRNA targeting HSP70 with HSA, holds promise for developing an effective and targeted therapy for cancer treatment. The incorporation of ICG and siRNA into HSA NPs allows for the precise co-delivery of these therapeutic agents to the tumor site, exploiting the unique properties of each component to synergistically enhance the efficacy of PTT (Figure 1B).

Material and Methods

Materials

HSA lyophilized powder was purchased from Beijing Biorigin Inc. Sodium Hydroxide (NaOH) and Anhydrous Ethanol from the Beijing Chemical Factory. 50% Glutaraldehyde was provided by Shanghai Maiklin Biochemical Technology Co., Ltd. ICG and BCA Protein Assay Kit was obtained from Thermo Fisher Scientific (USA). Phosphate Buffered Saline (PBS) was purchased from Beijing Noble Ryder Technology Co., Ltd. GelRed Nucleic Acid Gel Stain was procured from Biotium.Inc (USA) for

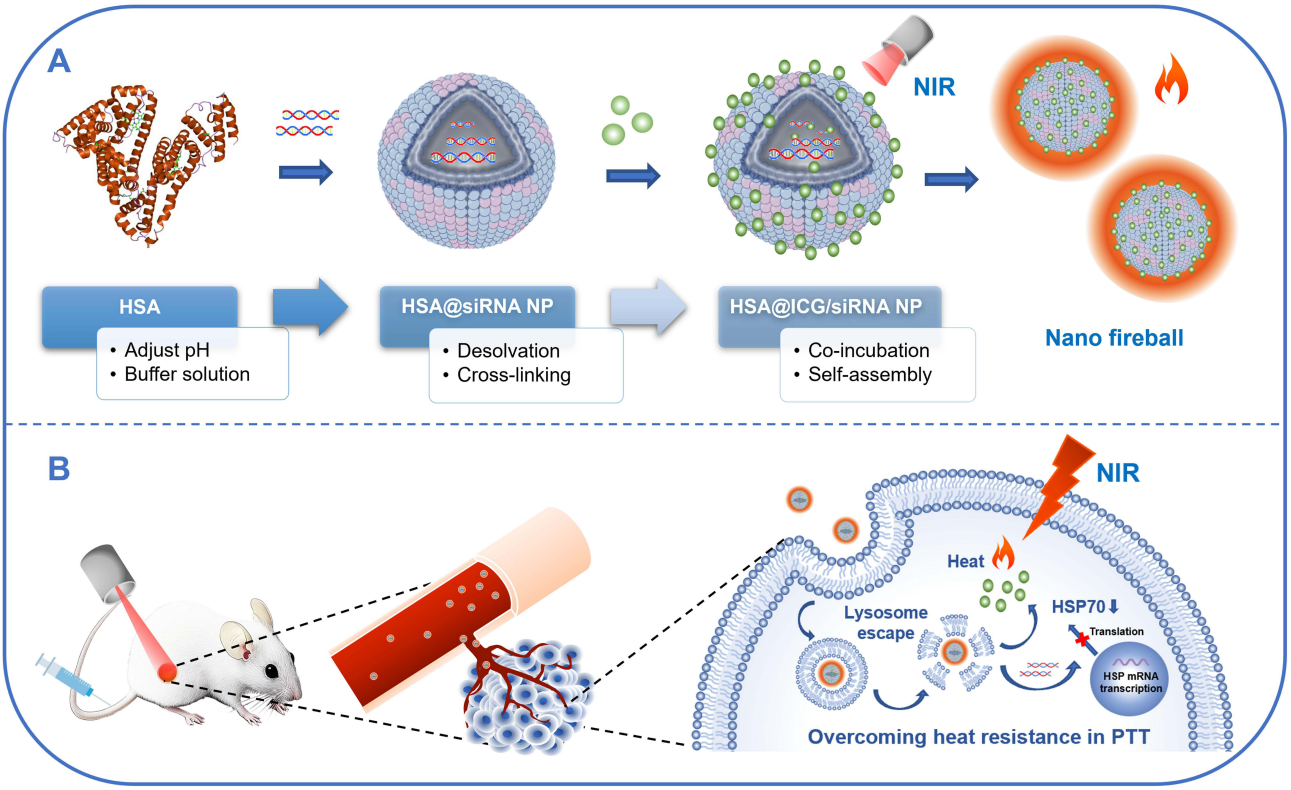

Figure 1 A schematic overview of HSA@ICG/siRNA NPs design and their anti-tumor efficacy. (**A**) The nanoparticles were synthesized via desolvation-crosslinking for siRNA encapsulation within HSA, followed by ICG loading through co-incubation and self-assembly. (**B**) Upon systemic administration, the nanoparticles accumulate at the tumor site. NIR irradiation induces photothermal heating, facilitating lysosomal escape of siRNA and downregulation of HSP70 expression, thereby enhancing the sensitivity of tumor cells to PTT and promoting cancer cell death.

visualizing nucleic acids. RNase was obtained from Sigma (USA). Ethylenediaminetetraacetic Acid (EDTA) was sourced from Solarbio (China). The Cell Counting Assay Kit (CCK-8) was acquired from Xinsaimi Biological Technology Co., Ltd. Thiazolyl Blue tetrazolium bromide (MTT, Aladdin, China). The sequences of HSP70 siRNA are 5′-CGCAGAACACCGUGUUCGA-3′ (sense) and 5′-UCGAACACGGUGUUCUGCG-3′ (anti-sense). Gene Pharmaceutical Technology Co., Ltd. (Shanghai, China) supplied the mouse-derived HSP70 siRNA-Cy5, the negative control HSP70 siRNA (NC), the probe HSP-70 customized gene qRT-PCR quantitative kit, and the GAPDH/β-actin calibration qRT-PCR quantitative kit.

The 4T1 cell line (mouse breast tumor cells) was obtained from the Cell Bank of the Chinese Academy of Sciences. Cells were cultured in RPMI-1640 medium supplemented with 10% fetal bovine serum (FBS) and 1% penicillin-streptomycin, and incubated at 37°C with 5% CO_2.

Specific pathogen-free female BALB/c mice (weighing 16–18 g) were purchased from the Beijing Vital River Laboratory Animal Technology Co., Ltd. The trial was conducted in accordance with the guidelines of the Capital Medical University Animal Welfare Ethics Committee (approval ID: AEEI-2023-047).

Synthesis of HSA@ICG NPs

At room temperature, 4 mg HSA powder was weighed and placed into a vial. Next, 200 μL of purified water was added, and the solution pH was adjusted to 10.8 using 1 mol/L NaOH solution. The mixture was stirred uniformly at 700 rpm on a thermostatic magnetic stirrer until the HSA was completely dissolved. Using a syringe pump, 0.8 mL of anhydrous ethanol was gradually added to the solution at a rate of 1.0 mL/min, resulting in a visible Tyndall effect. The solution was continuously stirred at room temperature to allow for the formation of albumin nanoparticles. After 3 hours, 5 μL of a 50% glutaraldehyde solution was added to the nanoparticles to induce crosslinking, with stirring continued at 700 rpm on a thermostatic magnetic stirrer for an additional 24 hours. The mixture was then centrifuged at 3000 rpm for 10 minutes at 4°C using a 100 kDa ultrafiltration tube, and the filtrate

https://doi.org/10.2147/IJN.S511655

was discarded. The retentate was washed with 1 mL of purified water and centrifuged again for 10 minutes, after which the filtrate was discarded, leaving the purified albumin NPs.

To load ICG, 200 μL of a prepared 4 mg/mL ICG solution was added to the albumin nanoparticles with thorough mixing. The reaction mixture was covered with aluminum foil to prevent light exposure and incubated overnight in a 37°C water bath shaker. Following incubation, the mixture was centrifuged at 3000 rpm for 10 minutes at 4°C using a 100 kDa ultrafiltration tube, and the filtrate was discarded. The resulting HSA@ICG NPs were resuspended in 1 mL of distilled water, and the final concentration was determined according to ICG UV absorption standard curves.

Synthesis of HSA@ICG/siRNA NPs

Initially, 4 mg HSA powder was weighed and placed into a vial. Next, 200 μL of purified water was added, and the solution pH was adjusted to 10.8 using 1 mol/L NaOH solution. The mixture was stirred uniformly at 700 rpm on a thermostatic magnetic stirrer until the HSA was completely dissolved. 3 μL of a 100 μM siRNA (siRNA-Cy3 or siRNA-Cy5) solution was added to the HSA solution, and the mixture was stirred at 700 rpm on a thermostatic magnetic stirrer for 15 minutes. Using a syringe pump, 0.8 mL of anhydrous ethanol was gradually added to the solution at a rate of 1.0 mL/min, resulting in a visible Tyndall effect. After 3 hours, 5 μL of a 50% glutaraldehyde solution was added to crosslink. The synthesis process was subsequently completed according to the method detailed in the HSA@ICG NPs synthesis section.

Characterization of HSA@ICG and HSA@ICG/siRNA NPs

The particle size and surface charge of NPs were measured using a zeta potential analyzer (ZS90, Malvern, USA). The morphology of both HSA@ICG and HSA@ICG/siRNA NPs was observed with transmission electron microscopy (TEM) (JEM 1230, JEOL, Japan). The fluorescence emission spectra of siRNA Cy3 and Cy5 were measured using a fluorescence spectrometer (F2500, HITACHI, Japan). The ultraviolet-visible (UV-vis) absorption spectra of ICG were obtained using a UV-vis spectrophotometer (UV 2600, Shimadzu, Japan). The temperature rise of the nanoparticles under varying power intensities and exposure times was monitored using an 808 nm infrared laser (Changchun Leirui Optoelectronics Technology Co., Ltd.) along with a thermal imager (FOTRIC, USA).

Encapsulation Efficiency and Drug Loading Capacity of ICG

To determine the encapsulation efficiency (EE%) and drug loading capacity (DLC%) of ICG, standard solutions were prepared at concentrations of 1.5625, 3.125, 6.25, 12.5, and 25 μg/mL. The absorbance of each solution was measured at 790 nm to generate a standard calibration curve. Subsequently, the absorbance of the prepared HSA@ICG/siRNA NPs solution was measured to determine the concentration of encapsulated ICG. The encapsulation efficiency and drug loading capacity were calculated using the following formulas:

$$\mathrm{EE\%} = \frac{\text{ICG content in NPs } (\mu\mathrm{g})}{\text{Total ICG input}(\ \mu\mathrm{g})} \times 100\%$$

$$\mathrm{DLC\%} = \frac{\text{ICG content in NPs } (\mu\mathrm{g})}{\text{HSA NPs yield } (\mu\mathrm{g})} \times 100\%$$

Encapsulation Efficiency and Drug Loading Capacity of siRNA HSP70

For the determination of siRNA HSP70 encapsulation efficiency and drug loading, standard solutions were prepared at concentrations of 0.001, 0.006, 0.012, 0.025, 0.05, 0.22, and 0.67 μg/mL. To create a standard curve, fluorescence measurements were conducted using a fluorescence spectrophotometer with excitation at 650 nm and emission at 670 nm. The fluorescence of the HSA @siRNA NP solution was then measured under the same excitation and emission conditions, allowing for calculating encapsulation efficiency and drug loading based on the established standard curve.

$$EE\% = \frac{\text{siRNA content in NPs } (\mu g)}{\text{Total siRNA input } (\mu g)} \times 100\%$$

$$DLC\% = \frac{\text{siRNA content in NPs } (\mu g)}{\text{HSA NPs yield } (\mu g)} \times 100\%$$

Anti-RNase A Degradation in Vitro

For the nuclease stability assay, naked siRNA and HSA@ICG/siRNA NPs samples, each containing 5 μL of 0.15 μM siRNA, were incubated with 2 μL of 10 μg/mL RNase A solution at 37°C. The reaction was terminated by adding 2 μL of 10 mg/mL EDTA solution at 0 and 0.5 hours for naked siRNA samples, and at 0, 0.5, 1, 2, and 4 hours for HSA@ICG/siRNA NPs. To release siRNA from NPs, 10 μL of 0.8 mg/mL heparin sodium was added 30 minutes before electrophoresis, followed by RNA loading buffer. 1% agarose gel prepared in TBE buffer and stained with GelRed was used for visualization. Gel electrophoresis was run at 100 V for 30 minutes, and siRNA bands were visualized using a ChemiDoc imaging system (Bio-Rad, USA).

HSP70 siRNA Release Experiment in vitro

To evaluate the siRNA release profile from HSA@ICG/siRNA NPs, dialysis bags with a 50 kDa molecular weight cutoff were filled with 200 μL of 0.15 μM HSA@ICG/siRNA NPs solution, either irradiated (1 W/cm² for 3 minutes) or non-irradiated, and sealed. The dialysis bags were rinsed with PBS and immersed in 5 mL of PBS within 10 mL centrifuge tubes, which were then placed in a 37°C light-protected water bath shaker. At predetermined intervals (1, 2, 3, 4, 6, 8, and 24 hours), 1 mL of the external phase PBS was sampled and replaced with fresh PBS. After 24 hours, the internal phase from each dialysis bag was collected, and the fluorescence intensities of siRNA in both the external and internal PBS phases were quantified using a fluorescence spectrophotometer. The cumulative siRNA release was calculated to assess the release kinetics.

Cellular Uptake and Lysosomal Escape

To assess cellular uptake of Cy3-labeled siRNA, 4T1 cells were seeded in confocal culture dishes and incubated for 48 hours at 37°C with 5% CO_2 to facilitate cell attachment and growth. After confirming cell adherence, the medium was replaced with a fresh medium containing either Naked siRNA or HSA@ICG/siRNA NPs at a final Cy3-siRNA concentration of 10 nM. The cells were incubated for another 4 hours under the same conditions for cellular uptake. Following incubation, the medium was discarded, and the cells were rinsed with PBS. Hoechst 33342 staining solution (4 μL, 4 μg/mL) was then added to each dish for nuclear staining, and the cells were incubated for 15 minutes.

To assess lysosomal escape, 4T1 cells were treated with Cy3-labeled siRNA as a control or HSA@ICG/siRNA nanoparticles, with all groups containing a final concentration of 10 nM Cy3-siRNA. After 8-hour incubation, one group of the HSA@ICG/siRNA NPs was irradiated with an 808 nm NIR laser at a power density of 0.76 W/cm² for 3 minutes. Following an additional 4-hour incubation, the cells were rinsed with PBS and stained with Hoechst 33342 (4 μL, 4 μg/mL) and Lysotracker Green (0.5 μL, 75 nM) to visualize lysosomes. Cellular localization and lysosomal escape were evaluated using confocal laser scanning microscopy (CLSM, TCSSP5, Germany).

Cell Viability and Cytotoxicity Assay

To assess cell safety evaluation, 4T1 cells were seeded in 96-well plates at a density of 8×10^3 cells per well and incubated at 37°C with 5% CO_2 for 24 hours to allow cell attachment. After confirming cell adherence, the test compounds HSA@ICG and HSA@ICG/siRNA NPs were added at concentrations of 5, 8, 10, 20, and 40 μg/mL. The cells were incubated with the test compounds for another 48 hours under the same conditions. Following this incubation, cell morphology was observed under a microscope. Then, CCK-8 solution was added to each well at a 1:10 dilution with the culture medium, and the plates were incubated for 1 hour. Finally, absorbance was measured at 450 nm using a microplate reader (Multiscan Spectrum 1500, Thermo, USA) to determine cell viability.

To evaluate cytotoxicity, 4T1 cells were seeded at a density of 8×10^3 cells per well in a 96-well plate and incubated at 37°C with 5% CO_2 for 24 hours to allow for cell attachment. After confirming cell adherence, varying concentrations of HSA@ICG and HSA@ICG/siRNA NPs (2, 10, and 30 μg/mL) were added to each well, and the cells were incubated under standard conditions for 8 hours. Following this incubation, each treated well was irradiated at 808 nm with an intensity of 0.76 W/cm² for 3 minutes and then returned to the incubator for 24 hours. Subsequently, 25 μL of a 5 mg/mL MTT working solution was added to each well, and the plate was shaken gently to ensure mixing. The cells were incubated in a 37°C, 5% CO_2 incubator for 4 hours. After this period, 150 μL of DMSO was added to dissolve the formazan crystals. Absorbance was measured at 570 nm using a microplate reader to determine the optical density (OD) in each well. Cell viability was calculated based on the OD values to assess cytotoxic effects.

Calcein AM/PI Staining for Apoptotic Cells

To evaluate the proportion of live and dead cells, 4T1 cells were seeded at a density of 1×10^4 cells per well in a 24-well plate and incubated at 37°C with 5% CO_2 for 24 hours to allow for cell attachment. After confirming cell adherence, cells were treated with HSA@ICG or HSA@ICG/siRNA NPs at a concentration of 30 μg/mL and incubated for 8 hours under standard conditions. Each treated well was irradiated at 808 nm with an intensity of 0.76 W/cm² for 3 minutes, followed by an additional 24-hour incubation. Following treatment, cells were stained with a Calcein AM/PI detection working solution (1:500) and incubated at 37°C for 20 minutes in the dark. Live cells stained with Calcein-AM displayed green fluorescence (E_x/E_m = 494/517 nm), while dead cells stained with PI showed red fluorescence (E_x/E_m = 535/617 nm), and were visualized by fluorescence microscopy.

Real-Time PCR

Real-time reverse transcription PCR was performed using a PCR system (9700, 7500, Thermo, USA). 4T1 cells were transfected with blank medium, naked siRNA, Lipo2000/siRNA, HSA@ICG/siRNA, and HSA@ICG/siRNA NPs with NIR irradiation, with a final HSP70 siRNA concentration of 10 nM. After 8 hours of incubation, the HSA@ICG/siRNA NPs group was irradiated at 808 nm with an intensity of 0.76 W/cm² for 3 minutes. Following an additional 24 hours of incubation, total RNA was extracted from each sample using Trizol reagent. RNA concentration and purity were assessed with NanoDrop spectrophotometer (NanoDrop 1000, Thermo, USA). 2 μg of RNA were reverse-transcribed into complementary DNA (cDNA) using a reverse transcription kit. The cDNA was subjected to PCR amplification with specific primers for the target gene HSP70, with GAPDH serving as the internal control. Relative expression levels of HSP70 mRNA were quantified using the $2^{-\Delta\Delta Ct}$ method.

Western Blot

4T1 cells were treated with either blank medium, naked siRNA, Lipo 2000/siRNA, or HSA@ICG/siRNA NPs with a final HSP70 siRNA concentration of 10 nM. After 8 hours of incubation, the HSA@ICG/siRNA NPs group was irradiated at 808 nm with an intensity of 0.76 W/cm² for 3 minutes. Following 48 hours of incubation, proteins were extracted from the cells using RIPA buffer on ice. Protein concentrations were measured using the BCA assay. Equal amounts of protein were denatured and loaded onto a 12% SDS-PAGE gel, followed by electrophoresis at 120 V for approximately 1 hour. Proteins were then transferred to a PVDF membrane pre-activated in methanol, using a transfer buffer and a current of 400 mA for 35 minutes on ice. The membrane was blocked with QuickBlock™ solution at room temperature for 2 hours, then incubated overnight at 4°C with primary antibodies specific to the target protein HSP70 and β-actin as a loading control. Following three washes with TBST, the membrane was incubated with HRP-conjugated secondary antibodies for 1 hour at room temperature. After additional TBST washes, protein bands were visualized using ECL reagent chemiluminescent reagent and imaged by imaging systems (ChemiDoc, Bio-Rad, USA).

Evaluation of the Photothermal Effect of HSA@ICG NPs in Vivo

Murine 4T1 breast tumor-bearing mice were randomly divided into two groups (n=3): PBS group and HSA@ICG NPs group. Each mouse in the PBS group received an intravenous injection of 50 μL PBS, while each mouse in the HSA@ICG NPs group received 200 μL of HSA@ICG NPs at a dose of 3 mg/kg. After 8 hours, tumors were irradiated

with an 808 nm laser at a power density of 1.91 W/cm² for 3 minutes. Temperature changes in both groups were monitored with an infrared thermal imager (FOTRIC, USA), capturing readings at 30-second intervals over the 3-minute irradiation period.

In Vivo Imaging

To evaluate the biodistribution and targeting ability of HSA@ICG/siRNA NPs, in vivo fluorescence imaging was conducted in 4T1 tumor-bearing BALB/c mice. The mice were administered intravenous injections of either free ICG or HSA@ICG/siRNA NPs at a dose of 3 mg/kg ICG. Fluorescence imaging was performed at 1, 3, 8, 24, and 48 hours post-injection using an in vivo imaging system (IVIS Spectrum, PerkinElmer Inc., USA). Following the final imaging session, all mice were euthanized, and major organs (heart, liver, spleen, lungs, and kidneys) as well as the tumors were harvested.

Ex vivo fluorescence imaging of the dissected organs was conducted at 48 hours post-injection to quantify the organ-specific accumulation of each formulation. Fluorescence distribution in the organs was recorded using the in vivo fluorescence imaging system.

Tumor Inhibition of HSA@ICG/siRNA NPs in Vivo

To assess the therapeutic efficacy of HSA@ICG/siRNA NPs in vivo, 20 BALB/c SPF mice received injections of a 4T1 cell suspension (2×10^6 cells/mL) into the right hip. Once the tumors grew to around 200 mm^3 (volume calculated as length × $width^2/2$), the tumor-bearing mice were randomly divided into 4 groups (n=5): PBS, HSA@siRNA (13.3 μg/kg), HSA@ICG NPs (containing 3 mg/kg ICG), and HSA@ICG/siRNA NPs (containing 3 mg/kg ICG and 13.3 μg/kg siRNA).

The treatments followed an induction-maintenance strategy. Eight hours after injection, mice in the HSA@ICG and HSA@ICG/siRNA NPs groups received an initial laser irradiation at 808 nm with a power density of 1.91 W/cm² for 3 minutes. Subsequent sessions retained the same drug dosage but reduced the laser power density to 0.76 W/cm² for 3 minutes. Each treatment cycle included a one-day regimen of injection and irradiation, followed by two days of rest. This cycle was repeated for a total of three treatment sessions. Tumor measurements were taken every other day to monitor the response to the treatment.

After 12 days, organs (heart, liver, spleen, lungs, and kidneys) and tumor tissues were excised for further evaluation. The primary tumors and major organs were collected for H&E staining, TUNEL assay and Ki-67 staining.

Statistical Analysis

Group differences were assessed using a two-sided Student's *t*-test or one-way ANOVA. Data are presented as means ± standard deviation (SD) from three independent experiments. Statistical significance was defined as *$p < 0.05$, **$p < 0.01$ indicating higher significance.

Results

Synthesis and Characterization of HSA@ICG/siRNA NPs

HSA NPs were prepared using the desolvation method.[52,53] The process involves mixing HSA with siRNA and ICG, and forming them into stable nanoparticles through cross-linking and co-incubation (Figure S1). As depicted in Figures 2A and 2C, the initial HSA NPs exhibited a mean nanoparticle size of 101.3 ± 0.55 nm and a zeta potential of −14.1 ± 1.26 mV. Following the incorporation of siRNA, the nanoparticle size increased slightly to 111.1 ± 0.26 nm, accompanied by a change in surface charge to −20.7 ± 0.72 mV. This increase in particle size and negative zeta potential, and fluorescence spectrum of HSA@siRNA-Cy3 (Cy5) (Figure S2 and S3) all suggests the successful loading of siRNA into the nanoparticles. Upon conjugation with ICG, the nanoparticle size remained relatively stable at 109.5 ± 0.14 nm, while the zeta potential exhibited a significant increase in negativity, reaching −25.4 ± 1.51 mV. The observed increase in surface charge negativity indicates effective decoration of the NPs with ICG, which is likely due to the additional negative charge contributed by the ICG molecules. TEM images reveal that both HSA@ICG NPs and HSA@ICG/siRNA NPs exhibit a uniform size distribution and uniform spherical morphology. These results demonstrate the consistency of the spherical nanoparticles throughout the preparation process (Figure 2B).

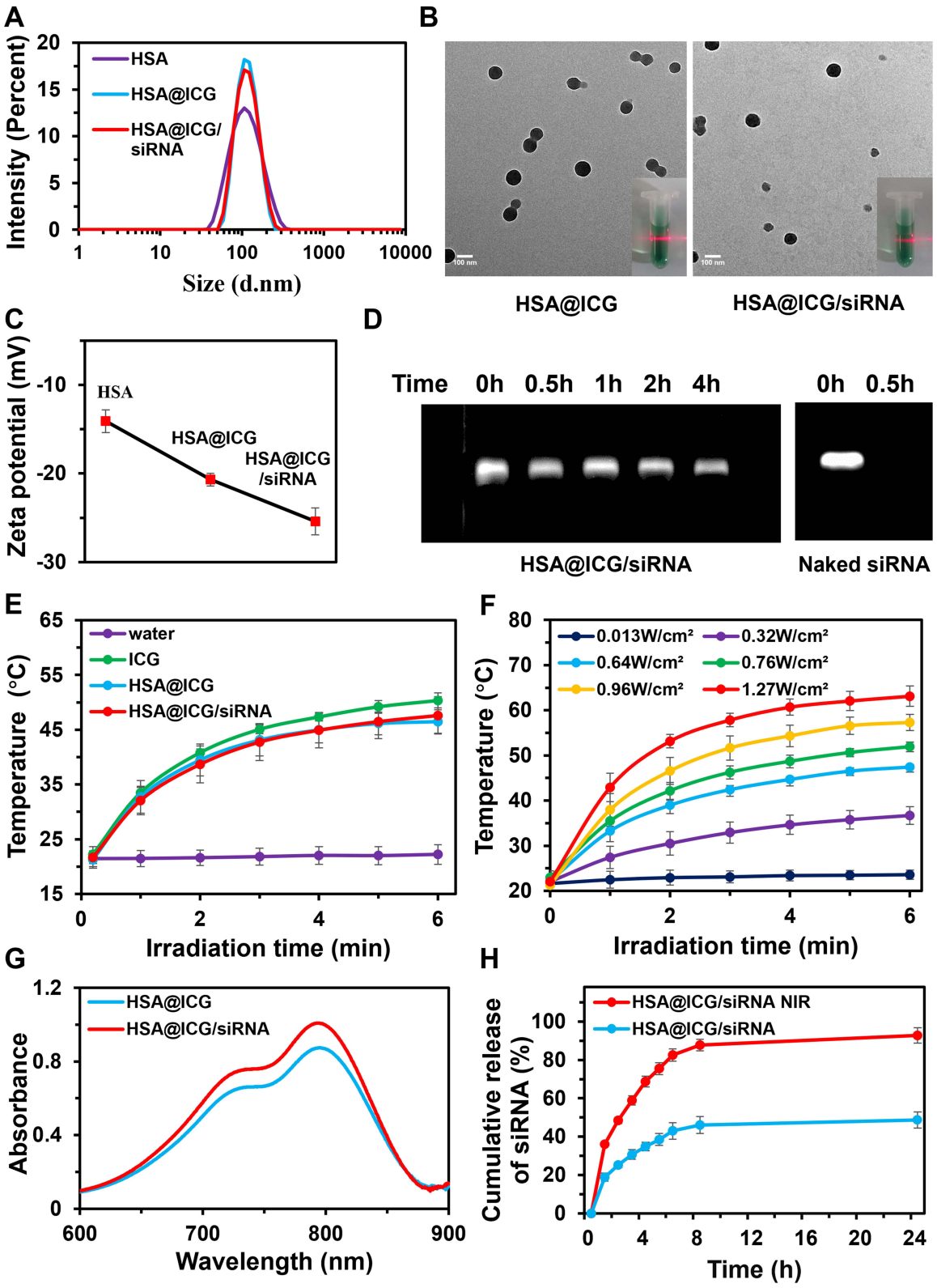

Figure 2 Characterization of physical and chemical properties of HSA@ICG/siRNA NPs. (**A**) DLS of HSA, HSA@ICG, HSA@ICG/siRNA NPs. (**B**) TEM images of the NPs and structure shape of HSA@ICG, HSA@ICG/siRNA NPS. (**C**) Zeta potential values of HSA, HSA@ICG, and HSA/ICG/siRNA NPs. The data were presented as the mean ± SD, n = 3. (**D**) Nuclease protection assay of HSA@ICG/siRNA NPs against RNase A. (**E**) Characterization of photothermal conversion of ICG, HSA@ICG, and HSA@ICG/siRNA NPs. The data were presented as the mean ± SD, n = 4. (**F**) Temperature variation curves of HSA@ICG/siRNA NPs under 808 nm laser irradiation at different power densities (0.013, 0.32, 0.64, 0.76, 0.96, 1.3 W/cm^2) for 1–6 min. The data were presented as the mean ± SD, n = 4. (**G**) UV-vis spectrum of HSA@ICG and HSA@ICG/siRNA NPs. (**H**) Cumulative release of HSA@ICG/siRNA NPs with irradiation and non-irradiation in a dialysis bag with a molecular weight of 50 k Da in PBS. The data were presented as the mean ± SD, n = 4.

The UV-vis absorbance spectra in Figure 2G suggested that the prepared HSA@ICG and HSA@ICG/ siRNA HSP70 are both complexes formed by conjugating ICG, respectively. ICG has a strong absorption peak of around 790 nm in the NIR region, making it suitable for photothermal therapy. According to the ICG UV absorption standard curve (Figure S4) and the absorbance of HSA@ICG/siRNA NPs, the encapsulation efficiency and drug loading capacity of ICG in HSA@ICG/siRNA NPs were determined to be 56.7% and 11.55%, respectively.

Based on the siRNA-Cy5 fluorescence standard curve (Figure S5) and the measured fluorescence intensities of HSA@ICG/siRNA NPs, the encapsulation efficiency of siRNA HSP70 was found to be 44.32%, with a drug loading capacity of 0.49 μg/mg, equivalent to 0.05%.

According to the BCA standard curve (Figure S6) and the absorbance of the supernatant from the HSA@ICG/siRNA NPs solution, the albumin NPs sphering rate was calculated to be 92.68%, indicating a high sphering efficiency.

Anti-RNase A Degradation in Vitro

The in vivo degradation of siRNA by RNase presents a significant challenge to the clinical application of siRNA therapies.[39] As demonstrated in Figure 2D, bands corresponding to naked siRNA disappeared after 0.5 hours of interaction with RNase A, indicating that RNAase A completely degrades naked siRNA. In contrast, the HSA@ICG/ siRNA NPs retained distinct bands after 4 hours of exposure to RNase A, suggesting that HSA nanoparticles effectively protect siRNA from RNase A degradation.

Photothermal Conversion Ability in Vitro

The temperature variation curves demonstrated a significant increase in temperature with increasing power densities during 808 nm laser irradiation. The comparative results showed that the photothermal conversion capacities of ICG, HSA@ICG, and HSA@ICG/siRNA NPs were basically consistent, with all formulations achieving temperatures of 46.5–50°C in 6 minutes (Figure 2E). Notably, at a power density of 0.76 W/cm² for 3 minutes, the temperature reached 46°C (Figure 2F). This indicates a strong photothermal effect at this power density. Further analysis was performed on temperature changes in samples with varying concentrations of ICG ranging from 0 to 30 μg/mL. At a consistent power density of 0.76 W/cm², higher concentrations resulted in higher temperatures, confirming that the photothermal conversion efficiency is concentration-dependent (Figure S7). The photothermal conversion efficiency of HSA@ICG/siRNA NPs was calculated to be 60.58% using an 808 nm near-infrared laser with a power density of 0.76 W/cm², demonstrating the efficacy of the nanoparticle system in converting light energy into heat for potential therapeutic applications. The intracellular photothermal conversion was assessed in 4T1 cells under similar laser irradiation conditions (808 nm, 0.76 W/cm² for 6 minutes). The results indicated that both HSA@ICG and HSA@ICG/ siRNA NPs achieved comparable temperatures of approximately 49°C within 3 minutes (Figure S8).

In vitro siRNA Release

As shown in Figure 2H, the release of siRNA was evaluated from HSA@ICG/siRNA NPs under both irradiated and non-irradiated conditions using fluorescence spectrophotometry. After 8 hours, the cumulative release percentages were 87.75% ± 0.14% for the irradiated group and 46.01% ± 0.20% for the non-irradiated group. Notably, the release of HSA@ICG/siRNA NPs was significantly enhanced following irradiation with an 808 nm laser (1 W/cm² for 3 minutes) compared to the non-irradiated condition. These results suggest that NIR irradiation effectively induces siRNA release.

Cellular Uptake and Lysosomal Escape

The 4T1 cells were exposed to either naked siRNA-Cy3 or HSA@ICG/siRNA NPs for 4 hours at a concentration of 10 nM. Subsequent staining with Hoechst 33342 and confocal microscopy revealed a striking difference in cellular uptake (Figure 3A). As expected, the control group treated with naked siRNA-Cy3 exhibited minimal to no red fluorescence within the cytoplasm, indicating negligible cellular uptake. Conversely, cells treated with HSA@ICG/siRNA NPs displayed a pronounced red fluorescence signal in the cytoplasmic compartment, clearly demonstrating the successful cellular uptake of siRNA.

Figure 3B illustrates the lysosomal escape of Cy3-labeled siRNA delivered via HSA@ICG/siRNA NPs, comparing conditions with and without NIR irradiation. Previous studies have demonstrated that NIR light can enhance nanoparticle lysosomal escape.[19,20] In confocal imaging, the non-irradiated HSA@ICG/siRNA NPs group exhibited weak and less

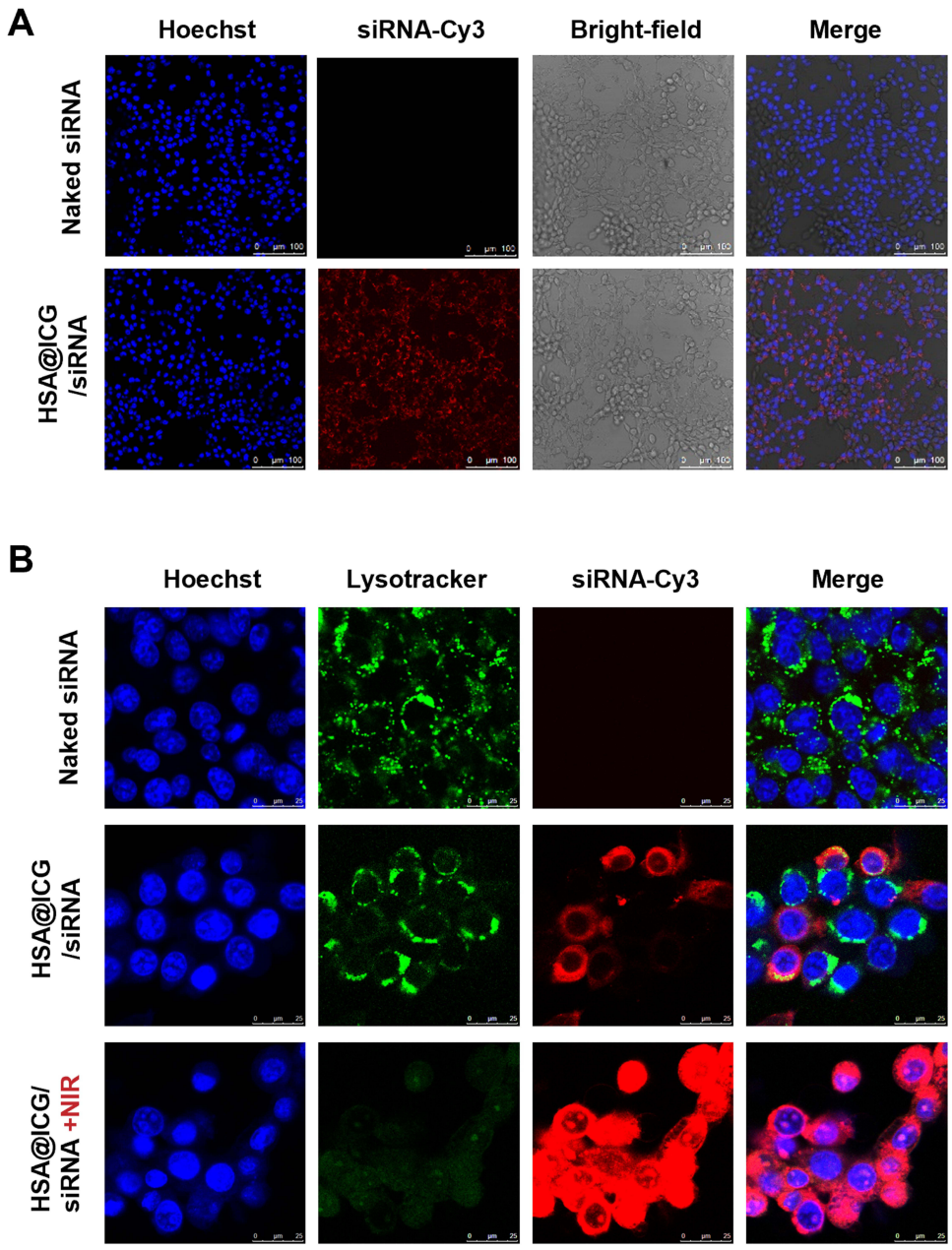

Figure 3 Cellular uptake and lysosomal escape visualized by confocal microscopy. (**A**)The confocal microscopy images illustrate the cellular uptake of Naked siRNA-Cy3 and HSA@ICG/siRNA NPs at a concentration of 10 nM for siRNA in 4T1 cells. (**B**) Confocal microscopy images of Cy3-labeled siRNA uptake in 4T1 cells treated with naked siRNA, HSA@ICG/siRNA NPs without irradiation, and HSA@ICG/siRNA NPs with 808 nm irradiation (0.76 W/cm², 3 min). Cells were stained with Hoechst (blue) for nuclei, Lysotracker (green) for lysosomes, and siRNA-Cy3 (red) for siRNA.

pronounced red fluorescence, indicating limited siRNA cytoplasmic release. Furthermore, the analysis revealed significant colocalization between Cy3 fluorescence (representing siRNA) and lysotracker green fluorescence (indicating lysosomes), suggesting that the nanoparticles were predominantly trapped within the lysosomal compartments. This entrapment could hinder effective siRNA delivery, as localization within lysosomes prevents the molecules from reaching their intracellular targets.

In contrast, NIR-irradiated cells showed higher siRNA fluorescence in the cytoplasm and a significant reduction in lysotracker fluorescence, further supporting the conclusion that NIR irradiation disrupts lysosomal integrity. These results suggest a potential escape of nanoparticles from the endosomal compartments, indicating enhanced cytoplasmic delivery of siRNA.

Cellular Viability and Cytotoxicity

The cell safety assay was conducted using CCK8 assay to evaluate the safety profile of HSA@ICG/siRNA NPs in 4T1 cells at different concentrations at 5, 8, 10, 20, 40 μg/mL without irradiation. Figure 4A illustrates that even at an ICG concentration of 40 μg/mL without laser irradiation, the cell survival rate remained above 90%, indicating the favorable cell safety of HSA@ICG/siRNA NPs.

To assess cytotoxicity, MTT assays were conducted on 4T1 cells treated with HSA@ICG and HSA@ICG/siRNA NPs at concentrations of 2, 10, and 30 μg/mL (Figure 4B). Upon irradiation at 808 nm, 0.76 W/cm² for 3 minutes, the two groups exhibited a notable increase in cytotoxicity with escalating concentrations. Comparatively, the cytotoxicity of HSA@ICG/siRNA NPs was higher than that of HSA@ICG NPs. At 30 μg/mL concentration, the cell viability for HSA@ICG was 37.4%, whereas for HSA@ICG/siRNA, it was 19.1%. This suggests that the incorporation of siRNA HSP70 effectively enhances the PTT efficacy, highlighting the potential of HSA@ICG/siRNA NPs for therapeutic applications.

Subsequently, the apoptotic morphology was evaluated using Calcein AM/PI staining and analyzed with fluorescence microscope. Figure 4C demonstrates varying degrees of damage among the blank control, blank control cells with NIR, HSA@ICG+NIR, and HSA@ICG/siRNA+NIR NPs groups. Notably, both the control and laser-irradiated cells exhibited minimal cytotoxicity. As expected, the HSA@ICG/siRNA NPs group, at a concentration of 30 μg/mL, demonstrated enhanced tumor-killing effects compared to the HSA@ICG NPs group under 808 nm NIR light irradiation.

Gene and Protein Expression

RT-PCR analysis was conducted to assess the gene silencing efficiency of HSA@ICG/siRNA NPs in 4T1 cells, using GAPDH as an internal control. Cells were treated with 10 nM HSP70 siRNA delivered via naked siRNA, Lipo2000/siRNA, and HSA@ICG/siRNA NPs with and without NIR irradiation. The $2^{-\Delta\Delta CT}$ method was employed to quantify relative mRNA levels of HSP70 across each treatment group. Results indicated that the gene silencing efficacy of HSA@ICG/siRNA NPs group with NIR irradiation was significantly higher than in the control groups, with a notable reduction in relative HSP70 mRNA expression to 17.17% ± 13.89% (Figure 4D). This demonstrates that NIR light synergistically enhances gene silencing. The Lipo2000 group showed a moderate reduction in HSP70 mRNA. Given the previously reported cytotoxic effects of Lipo2000 on cells, this potential toxicity might have influenced the experimental outcomes.[54,55] Conversely, the HSA@ICG/siRNA NPs group without irradiation exhibited a minor reduction. HSP70 expression is typically stress-induced.[56] Without stressors like NIR or cytotoxicity, baseline HSP70 levels might remain low, resulting in minimal differences in mRNA levels compared to control groups.

Western blotting was performed to assess the protein expressions of cellular HSP70, utilizing β-actin as the control. 4T1 cells underwent treatment with Naked siRNA, Lipo2000/siRNA, and HSA@ICG/siRNA NPs with NIR irradiation, each containing an equivalent concentration of 10 nM siRNA HSP70. The relative protein expression levels of HSP70 in response to Control, Naked siRNA, Lipo2000/siRNA, and HSA@ICG/siRNA+NIR NPs were determined to be 2:1.5:1.2:0.7, indicating a 65% reduction in HSP70 protein expression in the HSA@ICG/siRNA NPs group (Figure 4E). Following treatment, the protein levels of HSP70 in the HSA@ICG/siRNA NPs with irradiation group were significantly decreased compared to the control group, indicating effective gene silencing and reduced target protein expression.

Photothermal Effect and Biodistribution in Vivo

The photothermal effect of HSA@ICG NPs on a 4T1 tumor-bearing model in BALB/c mice was investigated with an infrared thermal imager. Mice were intravenously injected with PBS or HSA@ICG nanoparticles, and after 8h, both groups were irradiated with an 808 nm infrared laser at a power density of 1.91 W/cm² for 3 minutes. The photo images are captured every 30 seconds (Figure 5A). The temperature in the tumor region of HSA@ICG NPs treatment group reached 42.3°C within 3 minutes of laser irradiation, indicating an effective response suitable for mild photothermal treatment. In contrast, the PBS group exhibited only a slight temperature increase to 35.0°C, which was insufficient to exert tumor inhibitory effects. Figure 5B presents the temperature variation curves of the HSA@ICG NPs and PBS groups in vivo. The observed temperature

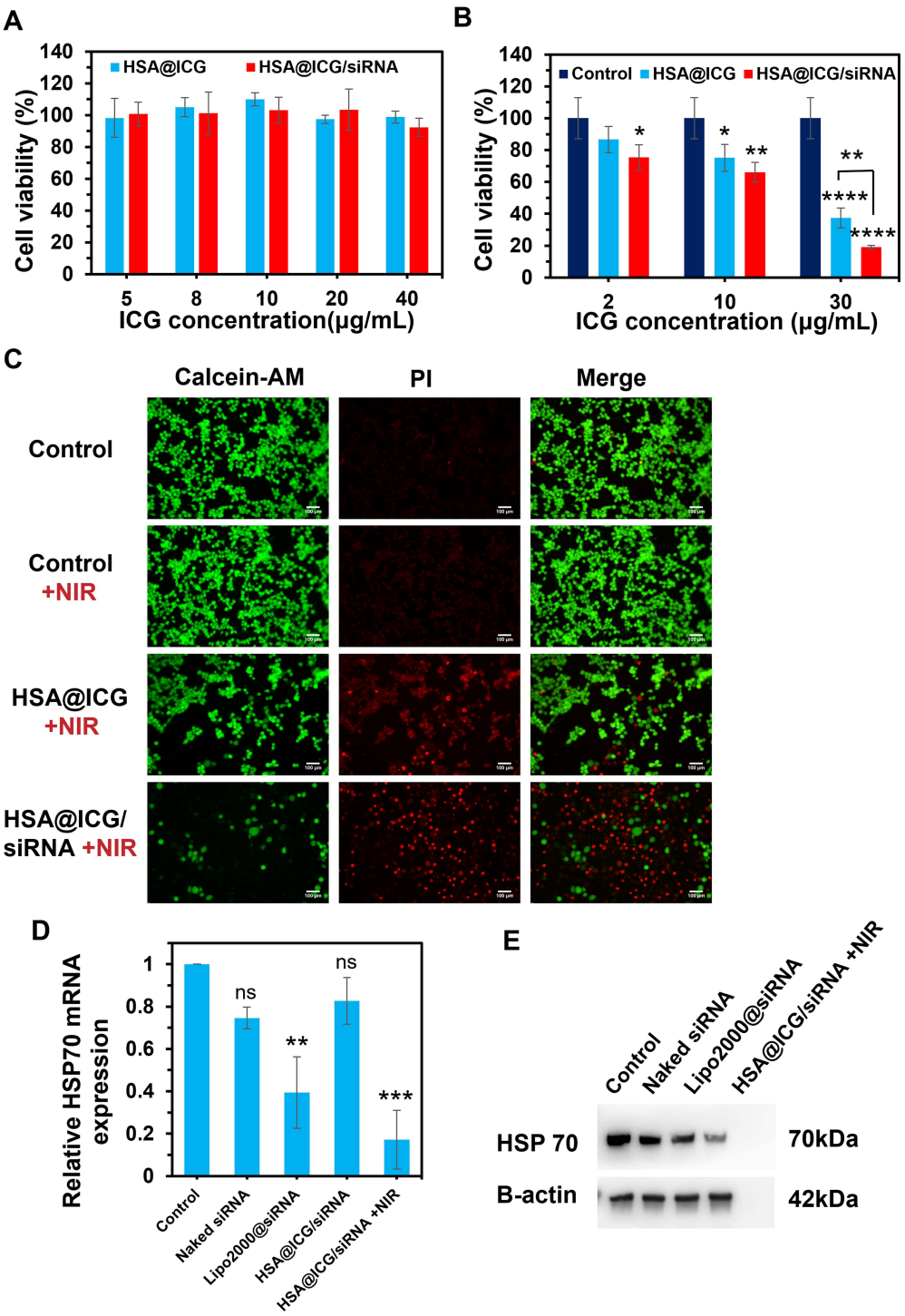

Figure 4 Effects of treatments on 4T1 cell cytotoxicity and HSP70 expression. (**A**) Cell viability of 4T1 cells treated with various concentrations of HSA@ICG, HSA@ICG/siRNA NPs without NIR exposure. The data are presented as means ± SD, n = 3. (**B**) Cell viability of 4T1 cells treated with various concentrations of HSA@ICG, HSA@ICG/siRNA NPs with laser irradiation (808 nm, 0.76 W /cm^2, 3 min). Data are presented as means ± SD, n=4, ****p < 0.0001, **p < 0.01, *p < 0.05. The data are presented as means ± SD, n = 3. (**C**) Confocal fluorescence images of Calcein AM/PI staining to distinguish between dead (red) and living cells (green) with esterase activity in 4T1 tumor cells after various treatments. The equivalent concentration of ICG was 30 μg/mL combined with laser irradiation (808 nm, 0.76 W /cm^2, 3 min). (**D**) Real-time qPCR method to amplify the cDNA of HSP70 siRNA formulations. At the same time, the GAPDH is used as the internal control. 4T1 cells were treated with Naked siRNA, Lipo2000/siRNA, and HSA@ICG/siRNA NPs+NIR irradiation (808 nm, 0.76 W / cm^2, 3 min), each containing the same amount of 10 nM of siRNA HSP70. (The $2^{-\Delta\Delta CT}$ method) Data are presented as means ± SD, n=4, **p < 0.01, ***p < 0.001. (**E**) Protein expression levels were assessed using Western blot assay specific to the target proteins, demonstrating the modulation of HSP70 protein levels in response to the treatment groups.

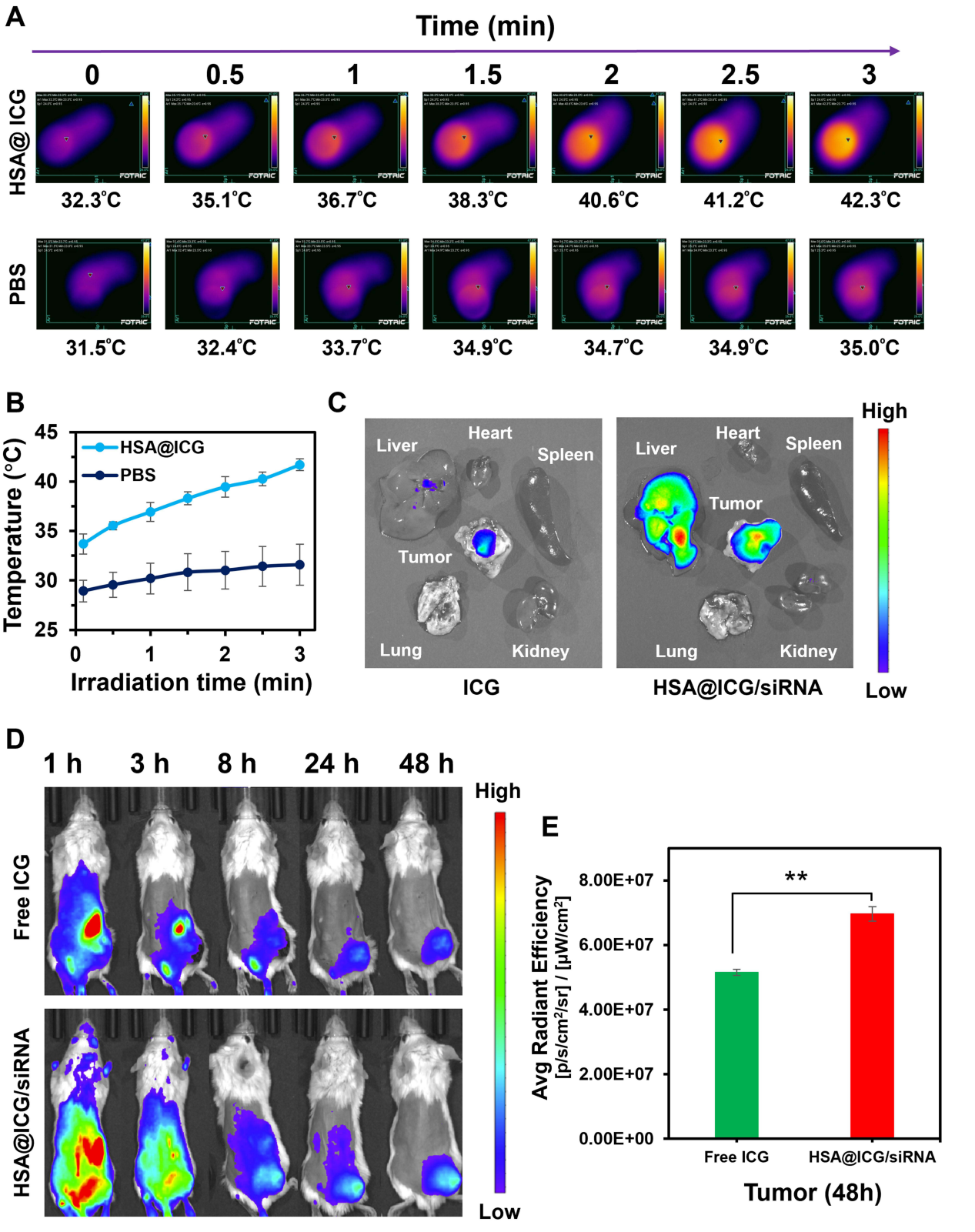

Figure 5 Thermal and fluorescence imaging of HSA@ICG/siRNA NPs for tumor targeting. (**A**) Thermal images of tumor-bearing mice treated with PBS or HSA@ICG NPs and irradiated with an 808 nm laser 3 min (1.91 W/cm²). (**B**) Temperature variation curves of tumor regions in mice treated with PBS or HSA@ICG NPs. The data were presented as the mean ± SD, n = 3. (**C**) Ex vivo fluorescence imaging of major organs and tumors was conducted 48 hours post-injection with free ICG or HSA@ICG/siRNA NPs. Organs were harvested from tumor-bearing BALB/c mice to evaluate biodistribution. (**D**) In vivo fluorescence imaging was performed on tumor-bearing BALB/c mice at 1, 3, 8, 24, and 48 hours post-injection with free ICG or HSA@ICG/siRNA NPs to monitor time-dependent biodistribution (n=4). (**E**) Quantitative analysis of fluorescence intensity in tumor in vivo at 48 hours post-injection, comparing free ICG and HSA@ICG/siRNA NPs groups. Data are presented as means ± SD, n=4, **p < 0.01.

https://doi.org/10.2147/IJN.S511655

increase in the HSA@ICG NPs group lies within a therapeutic range, suggesting its potential to induce tumor cell death while minimizing damage to surrounding healthy tissues.

To assess the biodistribution and clearance of HSA@ICG/siRNA NPs, we performed fluorescence imaging studies. The findings revealed that both free ICG and HSA@ICG/siRNA NPs accumulated in the tumor, with HSA@ICG/siRNA NPs showing significantly higher fluorescence intensity compared to free ICG (Figure 5D and E). Free ICG has a short circulation half-life and is rapidly cleared through the hepatobiliary excretion pathway, primarily via the liver.[57,58] However, it still demonstrates notable tumor accumulation, likely due to its affinity for serum albumin and high-density lipoproteins (HDLs) in the bloodstream.[59] This affinity transiently enhances its stability and circulation time, enabling passive tumor accumulation.[59,60]

Figure 5C shows the fluorescence intensity of various organs 48 hours after administration of free ICG or HSA@ICG/siRNA NPs. By 48 hours post-administration, as shown in ex vivo fluorescence imaging, most free ICG is likely metabolized and/or excreted, contributing to the lower fluorescence signal. The HSA@ICG/siRNA NPs exhibits markedly enhanced tumor accumulation compared to free ICG, suggesting improved tumor targeting.

Anti-Tumor Efficacy and Safety Evaluation in Vivo

In Figure 6A, a tumor-bearing mouse model was established through the subcutaneous inoculation of 4T1 cells at a concentration of 2×10^6 cells/mL. Mice were intravenously injected with PBS, HSA@siRNA, HSA@ICG, and HSA@ICG/siRNA NPs at a dosage of 3 mg/kg. At 8 hours post-injection, mice of the HSA@ICG and HSA@ICG/siRNA NPs groups received an initial laser irradiation at 808 nm with a power density of 1.91 W/cm² for 3 minutes, aiming to maximize the photothermal effect. Promising results were observed following the initial high-power treatment. After this adequate initial response, the treatment was transitioned to a maintenance phase involving low-power irradiation. This approach effectively sustained the therapeutic effects while minimizing potential side effects. Thus, subsequent treatments maintained the same drug dose but reduced the laser power density to 0.76 W/cm² for 3 minutes. Each treatment group consisted of 5 mice, and three treatment sessions were conducted.

Figure 6B shows images of excised tumors, illustrating a visible reduction in tumor size in the treatment groups compared to the control group. Tumor weights at the study endpoint indicated a significant reduction in tumor mass in the HSA@ICG (50.00% ± 9.16%) and HSA@ICG/siRNA NPs (71.26% ± 7.92%) groups compared to the control group (Figure 6C).

Tumor growth rates were notably slower in the HSA@ICG and HSA@ICG/siRNA NPs groups relative to the control and HSA@siRNA groups, as shown in the tumor volume growth curves (Figure 6D) and visible mice photos (Figure S9).

Figure 6E shows histological analysis using H&E staining and TUNEL assays, revealing decreased tumor cell density and increased apoptosis in the HSA@ICG and HSA@ICG/siRNA NPs groups. TUNEL assays demonstrated higher levels of apoptosis in these groups, with apoptotic-positive 4T1 cells marked by green staining. These findings confirm the efficacy of HSA@ICG/siRNA NPs treatment in promoting apoptosis in tumor cells. The marked decrease in Ki-67 expression following HSA@ICG/siRNA NPs treatment signifies a substantial inhibition of tumor cell proliferation, reaffirming the formulation's anti-tumor efficacy.

Additionally, H&E staining of major organs (heart, liver, spleen, lungs, and kidneys) showed no significant pathological changes across the four experimental groups (Figure S10) and body weight data (Figure S11), indicating that the nano-drug delivery system and irradiation strategy did not produce notable toxicity in major organs in vivo. Overall, these results indicate a synergistic effect of PTT combined with siRNA delivery, leading to substantial tumor growth inhibition and increased apoptosis in tumor cells.

Discussion

The findings of this study demonstrate that HSA@ICG/siRNA NPs significantly enhance PTT efficacy in tumor cells by leveraging dual mechanisms: photothermal conversion and siRNA-mediated gene silencing. Characterization confirmed the successful synthesis of stable HSA@ICG/siRNA NPs with a negative charge, optimal size for efficient cellular uptake, and concentration-dependent photothermal conversion capability. The negative zeta potential of the nanoparticles is crucial for stability and biocompatibility, as it reduces particle aggregation and minimizes interactions with non-targeted cells.[61]

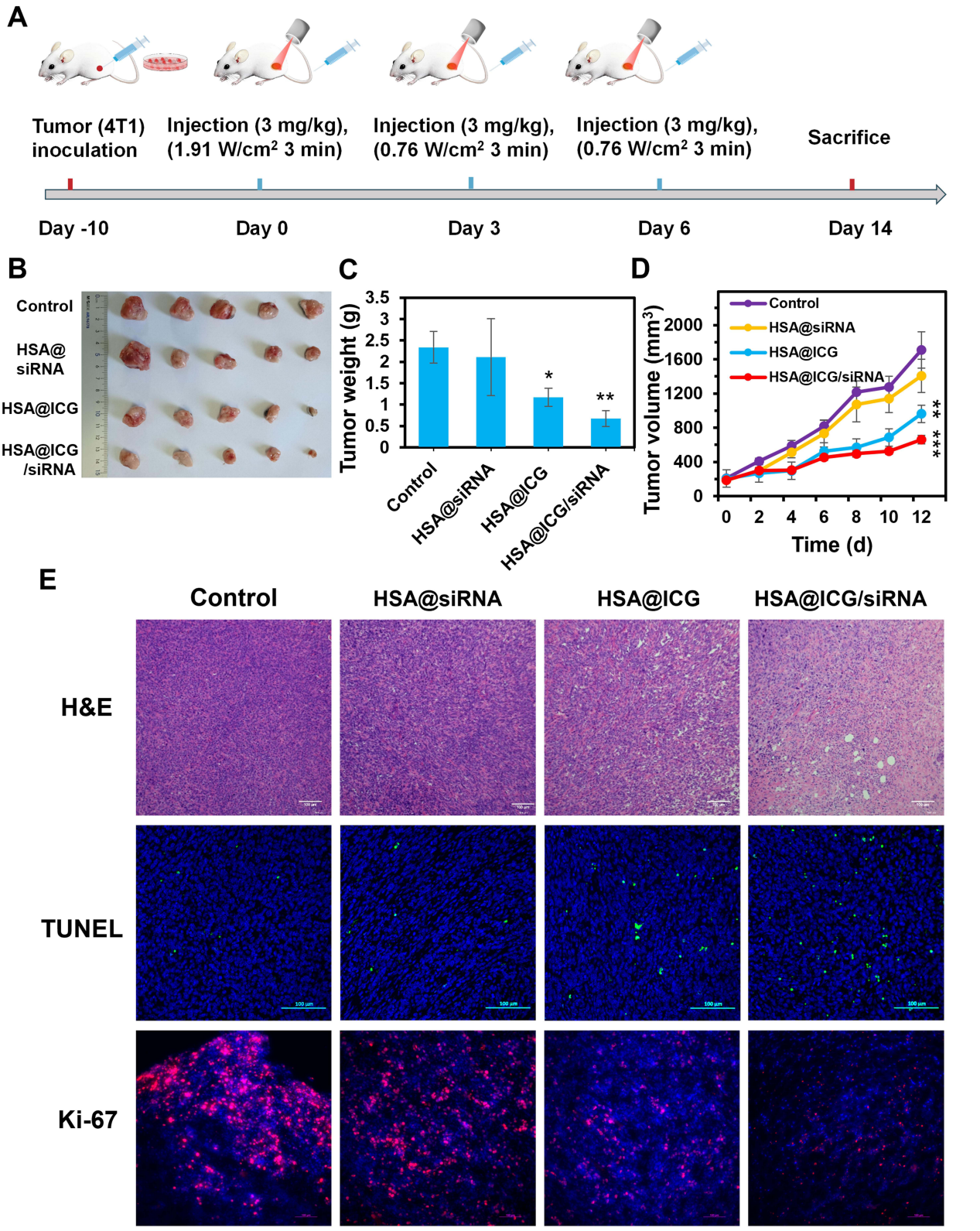

Figure 6 Anti-tumor therapeutic efficacy of PTT in 4T1 tumor-bearing BALB/c mice following injections of PBS, HSA@siRNA, HSA@ICG, and HSA@ICG/siRNA NPs at doses 3 mg/kg. (**A**) Timeline of drug administration and NIR irradiation in the tumor-bearing mouse model. (**B**) The photos of tumors were harvested concurrently at the study endpoint on Day 14. (**C**) Tumor weight at endpoint, data presented as mean ± SD, n=5, *p < 0.05, **p < 0.01. (**D**) Tumor volume growth curves, changes recorded every 2 days, ± SD, n=5, **p < 0.01, ***p < 0.001. (**E**) Histological analysis of 4T1 tumor tissues from mice treated with HSA@ICG/siRNA NPs, showing H&E staining for morphology, TUNEL assay for apoptosis, and Ki-67 immunofluorescence for proliferation. Scale bar: 100 μm.

https://doi.org/10.2147/IJN.S511655

The in vitro release study highlighted the potential of NIR-triggered release mechanisms for achieving efficient siRNA delivery. The mild hyperthermia destabilizes nanoparticle structures and may accelerate the release of encapsulated ICG and siRNA at the tumor site. Further investigations revealed high cellular uptake of siRNA and effective cytoplasmic delivery, leading to significant reductions in HSP70 expression at both the gene and protein levels. Several factors may influence gene and protein expression in this multifunctional nanoparticle system, particularly under stress response conditions. HSP70, a stress-induced protein, is upregulated during stimuli like NIR exposure and cytotoxic stress. Studies have shown that irradiation increases HSP70 levels due to heightened cellular stress.[17,24] Initial NIR exposure likely elevates HSP70 expression, followed by siRNA-mediated silencing. Furthermore, gene silencing results not only from siRNA specifically targeting HSP70 but also from cellular damage potentially induced by NIR exposure, highlighting the complex interplay of stress and therapeutic mechanisms.

Interestingly, despite our nanoparticles having a negative surface charge, we observed excellent cellular uptake, with a high internalization rate in 4T1 cells. This finding contradicts the common notion that positively charged nanoparticles exhibit better cellular uptake due to electrostatic interactions.[62,63] The efficient uptake of our negatively charged nanoparticles suggests the involvement of alternative uptake mechanisms. Although gp60, SPARC receptor-mediated endocytosis and passive diffusion have been extensively studied,[64–66] the nutrient-rich properties of albumin may further enhance nanoparticle internalization in tumor cells. A potential therapeutic strategy also has been proposed to improve the effectiveness of nanoparticulate HSA-bound drugs in cancer treatment by reprogramming nutrient signaling pathways and promoting macropinocytosis in cancer cells.[67] These findings underscore the efficacy of HSA@ICG/siRNA NPs in facilitating siRNA internalization, suggesting their potential as promising carriers for therapeutic siRNA delivery.

Previous studies have demonstrated that mild photothermal heating can enhance nanoparticle uptake by increasing cell membrane permeability and promoting cellular internalization.[18,68] In Figure 3B, a significant difference in total siRNA red fluorescence is observed between the laser and non-laser groups. This difference may be attributed to enhanced cellular uptake resulting from hyperthermia-induced changes in membrane permeability and improved lysosomal escape, leading to higher levels of detectable cytoplasmic siRNA.

The role of NIR-triggered lysosomal escape was particularly noteworthy, as the photothermal effect induced by NIR irradiation promoted lysosomal rupture, thus improving siRNA cytoplasmic release. ICG-mediated photothermal conversion generates heat and reactive oxygen species (ROS), both of which contribute to lysosomal destabilization. ROS-induced hydroxyl radicals damage lysosomal membranes, leading to rupture and enhanced siRNA release.[69–71]

Additionally, HSP70 downregulation plays a key role in further sensitizing lysosomal membranes to hyperthermia-induced rupture. HSP70 is known to maintain lysosomal integrity through interactions with lysosome-associated membrane protein 1/2 (LAMP1/2), lysosomal integral membrane protein 2 (LIMP2), and cluster of differentiation 63 (CD63), and its silencing weakens this protective function.[72] This enhanced delivery mechanism is crucial for maximizing the bioavailability of siRNA for cytoplasm delivery to target mRNA HSP70.

The in vivo biodistribution and photothermal studies further validated the efficacy. HSA@ICG/siRNA NPs demonstrated superior tumor accumulation and retention compared to free ICG, attributed to both passive and active targeting facilitated by the enhanced permeability and retention (EPR) effect and albumin receptor-mediated uptake.[64,73,74] Furthermore, mild hyperthermia can increase blood flow and vascular permeability, promoting nanoparticle accumulation and drug penetration.[75]

The significant reductions in tumor mass observed in the HSA@ICG/siRNA NPs group underscore the enhanced antitumor efficacy of the combined PTT and siRNA delivery system. The incorporation of siRNA appears to potentiate the therapeutic effects of PTT, likely through the silencing of the expression of HSP70, which is known to mitigate tumor cell resistance to thermal treatment.[76,77] This treatment followed the induction-maintenance strategy commonly employed in cancer therapies.[78] The initial high-dose laser irradiation phase achieved a robust therapeutic response via enhanced photothermal conversion. Subsequent adjustments in laser power density, the lower-power maintenance phase effectively sustained photothermal effects without compromising safety, illustrating the potential of dose-modified PTT protocols to balance therapeutic efficacy with minimized side effects.

In summary, this study presents HSA@ICG/siRNA NPs as a compelling strategy for integrating gene silencing and PTT, addressing the limitations of traditional PTT. These nanoparticles show promise as a multifunctional platform for

targeted, synergistic cancer therapy with potential clinical applicability. Future work could explore further optimization and evaluate the efficacy of HSA@ICG/ siRNA NPs across diverse tumor models to expand its therapeutic scope.

Conclusion

In summary, this study explored the role of siRNA in targeting HSP expression within the context of photothermal therapy. We developed HSA@ICG/siRNA nanoparticles to deliver siRNA specifically targeting HSP70 while incorporating the photothermal agent ICG. This study successfully demonstrates the synthesis and characterization of HSA@ICG/siRNA NPs, highlighting their promising applications in PTT for breast tumor treatment.

By leveraging the synergistic effects of siRNA-mediated HSP70 inhibition and ICG-based photothermal conversion, the HSA@ICG/siRNA nanoparticle system achieved significant cell cytotoxicity, effective gene silencing, and thermal ablation, while also promoting cellular uptake and lysosomal escape of siRNA. Furthermore, NIR light synergistically enhances siRNA functions by facilitating release and triggering lysosomal escape, thereby promoting effective gene silencing.

In vivo experiments confirmed improved tumor targeting, photothermal conversion, and prolonged retention of HSA@ICG/siRNA at the tumor site, resulting in effective tumor growth inhibition with minimal off-target toxicity.

Overall, the HSA@ICG/siRNA NP system represents a promising strategy for overcoming the limitations of traditional PTT by integrating gene silencing with targeted photothermal treatment.

Future research should focus on optimizing nanoparticle composition and investigating the broader applicability of this approach across various tumor types, thereby advancing its potential for clinical applications in cancer therapy.

Ethics Approval and Informed Consent

The trial was conducted in accordance with the guidelines of the Capital Medical University Animal Welfare Ethics Committee (approval ID: AEEI-2023-047).

Author Contributions

All authors contributed significantly to the work, including conception, study design, data acquisition, analysis, and interpretation. They participated in drafting, revising, or critically reviewing the article, gave final approval for the version to be published, agreed on the journal submission, and take responsibility for all aspects of the work.

Funding

This work was supported by the National Natural Science Foundation of China (81502688, 82304390), Cooperation Research Funding of Capital Medical University (2020KJ000514), Cooperation Research Funding of Capital Medical University (2023KJ000814), R&D Program of Beijing Municipal Education Commission (KM202210025024).

Disclosure

The authors declare no conflicts of interest.

References

1. Han B, Zheng R, Zeng H, et al. Cancer incidence and mortality in China, 2022. *J Nat Cancer Center*. 2024;4(1):47–53. doi:10.1016/j.jncc.2024.01.006
2. Siegel RL, Miller KD, Wagle NS, Jemal A. Cancer statistics, 2023. *CA Cancer J Clin*. 2023;73(1):17–48. doi:10.3322/caac.21763
3. Karanam NK, Story MD. An overview of potential novel mechanisms of action underlying tumor treating fields-induced cancer cell death and their clinical implications. *Int J Radiat Biol*. 2021;97(8). doi:10.1080/09553002.2020.1837984
4. Gottesman MM. Mechanisms of cancer drug resistance. *Annu Rev Med*. 2002;53(1):615–627. doi:10.1146/annurev.med.53.082901.103929
5. Farzam OR, Mehran N, Bilan F, et al. Nanoparticles for imaging-guided photothermal therapy of colorectal cancer. *Heliyon*. 2023;9(11). doi:10.1016/j.heliyon.2023.e21334
6. Jing Z, Du Q, Zhang X, Zhang Y. Nanomedicines and nanomaterials for cancer therapy: progress, challenge and perspectives. *Chem Eng J*. 2022;446. doi:10.1016/j.cej.2022.137147
7. Overchuk M, Weersink RA, Wilson BC, Zheng G. Photodynamic and photothermal therapies: synergy opportunities for nanomedicine. *ACS Nano*. 2023;17(9):7979–8003. doi:10.1021/acsnano.3c00891

8. Yang W, Liang H, Ma S, Wang D, Huang J. Gold nanoparticle based photothermal therapy: development and application for effective cancer treatment. *Sustainable Mat Technol*. 2019;22:e00109
9. Wang H, Li X, Tse BWC, et al. Indocyanine green-incorporating nanoparticles for cancer theranostics. *Theranostics*. 2018;8(5):1227–1242. doi:10.7150/thno.22872
10. Jung HS, Verwilst P, Sharma A, Shin J, Sessler JL, Kim JS. Organic molecule-based photothermal agents: an expanding photothermal therapy universe. *Chem Soc Rev*. 2018;47(7):2280–2297. doi:10.1039/c7cs00522a
11. Campu A, Focsan M, Lerouge F, et al. ICG-loaded gold nano-bipyramids with NIR activatable dual PTT-PDT therapeutic potential in melanoma cells. *Colloids Surf B Biointerfaces*. 2020:194. doi:10.1016/j.colsurfb.2020.111213.
12. Yoon HK, Ray A, Koo Lee YE, Kim G, Wang X, Kopelman R. Polymer-protein hydrogel nanomatrix for stabilization of indocyanine green towards targeted fluorescence and photoacoustic bio-imaging. *J Mater Chem B*. 2013;1(41):5611–5619. doi:10.1039/c3tb21060j
13. Thankachan D, Anbazhagan R, Tsai HC, et al. Enhanced tumor targeting with near-infrared light-activated indocyanine green encapsulated in covalent organic framework for combined photodynamic therapy (PDT) and photothermal therapy (PTT). *Dyes Pigm*. 2024;221:111812. doi:10.1016/j.dyepig.2023.111812
14. Chen S, Zhu L, Du Z, et al. Polymer encapsulated clinical ICG nanoparticles for enhanced photothermal therapy and NIR fluorescence imaging in cervical cancer. *RSC Adv*. 2021;11(34):20850–20858. doi:10.1039/d1ra02875h
15. Faria GNF, Karch CG, Chakraborty S, et al. Immunogenic treatment of metastatic breast cancer using targeted carbon nanotube mediated photothermal therapy in combination with anti-programmed cell death protein-1. *J Pharmacol Exp Ther*. 2024;390(1):65–77. doi:10.1124/jpet.123.001796
16. Li N, Dong F, Sun L, et al. Carrier-free delivery of nucleic acid and photosensitizer nanoparticles for enhanced photodynamic and gene antitumour therapy. *Fundam Res*. 2024;2024:1doi:10.1016/j.fmre.2024.03.014
17. Zhang B, Shao CW, Zhou KM, et al. A NIR-triggered multifunctional nanoplatform mediated by Hsp70 siRNA for chemo-hypothermal photothermal synergistic therapy. *Biomater Sci*. 2021;9(19):6501–6509. doi:10.1039/d1bm01006a
18. Chen Q, Liang C, Wang C, Zhuang L. An imagable and photothermal "Abraxane-like" nanodrug for combination cancer therapy to treat subcutaneous and metastatic breast tumors. *Adv Mater*. 2015;27(5):903–910. doi:10.1002/adma.201404308
19. Ye Q, Wang J, Guo R, et al. Enhancing antitumor efficacy of NIR-I region zinc phthalocyanine@upconversion nanoparticle through lysosomal escape and mitochondria targeting. *J Photochem Photobiol B*. 2024:255. doi:10.1016/j.jphotobiol.2024.112923.
20. Xiong H, Song Z, Wang T, et al. Photoswitchable dynamics and RNAi synergist with tailored interface and controlled release reprogramming tumor immunosuppressive niche. *Biomaterials*. 2025:312. doi:10.1016/j.biomaterials.2024.122712.
21. Yang X, Fan B, Gao W, et al. Enhanced endosomal escape by photothermal activation for improved small interfering RNA delivery and antitumor effect. *Int J Nanomed*. 2018;13:4333–4344. doi:10.2147/IJN.S161908
22. Liu Y, Bhattarai P, Dai Z, Chen X. Photothermal therapy and photoacoustic imaging: via nanotheranostics in fighting cancer. *Chem Soc Rev*. 2019;48(7):2053–2108. doi:10.1039/c8cs00618k
23. Jiang Z, Li T, Cheng H, et al. Nanomedicine potentiates mild photothermal therapy for tumor ablation. *Asian J Pharm Sci*. 2021;16(6):738–761. doi:10.1016/j.ajps.2021.10.001
24. Wu S, Gao M, Chen L, et al. A multifunctional nanoreactor-induced dual inhibition of HSP70 strategy for enhancing mild photothermal/chemodynamic synergistic tumor therapy. *Adv Healthc Mater*. 2024;13(23):2400819. doi:10.1002/adhm.202400819
25. Wang P, Chen B, Zhan Y, et al. Enhancing the efficiency of mild-temperature photothermal therapy for cancer assisting with various strategies. *Pharmaceutics*. 2022;14(11). doi:10.3390/pharmaceutics14112279
26. Jego G, Hazoumé A, Seigneuric R, Garrido C. Targeting heat shock proteins in cancer. *Cancer Lett*. 2013;332(2):275–285. doi:10.1016/j.canlet.2010.10.014
27. Lang BJ, Prince TL, Okusha Y, Bunch H, Calderwood SK. Heat shock proteins in cell signaling and cancer. *Biochim Biophys Acta mol Cell Res*. 2022;1869(3). doi:10.1016/j.bbamcr.2021.119187
28. Matokanovic M, Barisic K, Filipovic-Grcic J, Maysinger D. Hsp70 silencing with siRNA in nanocarriers enhances cancer cell death induced by the inhibitor of Hsp90. *Eur J Pharm Sci*. 2013;50(1):149–158. doi:10.1016/j.ejps.2013.04.001
29. Zhao K, Zhou G, Liu Y, et al. HSP70 family in cancer: signaling mechanisms and therapeutic advances. *Biomolecules*. 2023;13(4). doi:10.3390/biom13040601
30. Calderwood SK, Gong J. Heat shock proteins promote cancer: it's a protection racket. *Trends Biochem Sci*. 2016;41(4):311–323. doi:10.1016/j.tibs.2016.01.003
31. Xiao G, Zhao Y, Wang X, Zeng C, Luo F, Jing J. Photothermally sensitive gold nanocage augments the antitumor efficiency of immune checkpoint blockade in immune "cold" tumors. *Front Immunol*. 2023;14. doi:10.3389/fimmu.2023.1279221
32. Xin Y, Sun Z, Liu J, et al. Nanomaterial-mediated low-temperature photothermal therapy via heat shock protein inhibition. *Front Bioeng Biotechnol*. 2022;10. doi:10.3389/fbioe.2022.1027468
33. Lin J, Wang X, Ni D, Chen Y, Chen C, Liu Y. Combinational gene therapy toward cancer with nanoplatform: strategies and principles. *ACS Mat Au*. 2023;3(6):584–599. doi:10.1021/acsmaterialsau.3c00035
34. Ding F, Gao X, Huang X, et al. Polydopamine-coated nucleic acid nanogel for siRNA-mediated low-temperature photothermal therapy. *Biomaterials*. 2020;245:119976. doi:10.1016/J.BIOMATERIALS.2020.119976
35. Sun R, Wang Y, Sun Q, et al. MMP-2 responsive gold nanorods loaded with HSP-70 siRNA for Enhanced photothermal tumor therapy. *mol Pharm*. doi:10.1021/acs.molpharmaceut.4c00188
36. Zhang J, Wang Y, Zhu P, Wang X, Lv M, Feng H. SiRNA-mediated silence of protease-activated receptor-1 minimizes ischemic injury of cerebral cortex through HSP70 and MAP2. *J Neurol Sci*. 2012;320(1–2):6–11. doi:10.1016/j.jns.2012.05.040
37. Kim BS, Kumar D, Park CH, Kim CS. HSPA1A-siRNA nucleated gold nanorods for stimulated photothermal therapy through strategic heat shock to HSP70. *Mater Chem Front*. 2021;5(17):6461–6470. doi:10.1039/d1qm00630d
38. Shao L, Li Q, Zhao C, et al. Auto-fluorescent polymer nanotheranostics for self-monitoring of cancer therapy via triple-collaborative strategy. *Biomaterials*. 2019;194:105–116. doi:10.1016/j.biomaterials.2018.12.021
39. Wang Y, Chen S, Yang X, Zhang S, Cui C. Preparation optimization of bovine serum albumin nanoparticles and its application for siRNA delivery. *Drug Des Devel Ther*. 2021;15:1531–1547. doi:10.2147/DDDT.S299479

40. Li J, Wang S, Fontana F, et al. Nanoparticles-based phototherapy systems for cancer treatment: current status and clinical potential. *Bioact Mater*. 2023;23:471–507. doi:10.1016/j.bioactmat.2022.11.013
41. Shen X, Liu X, Li T, et al. Recent advancements in serum albumin-based nanovehicles toward potential cancer diagnosis and therapy. *Front Chem*. 2021:9. doi:10.3389/fchem.2021.746646.
42. Man XY, Sun ZW, Li SH, et al. Development of a Pt(II) compound based on indocyanine green@human serum albumin nanoparticles: integrating phototherapy, chemotherapy and immunotherapy to overcome tumor cisplatin resistance. *Rare Metals*. 2024;43(11):6006–22. doi:10.1007/s12598-024-02759-w
43. Jang HJ, Song MG, Park CR, et al. Imaging of indocyanine green-human serum albumin (ICG-HSA) complex in secreted protein acidic and rich in cysteine (SPARC)-expressing glioblastoma. *Int J Mol Sci*. 2023;24(1). doi:10.3390/ijms24010850
44. Lomis N, Westfall S, Farahdel L, Malhotra M, Shum-Tim D, Prakash S. Human serum albumin nanoparticles for use in cancer drug delivery: process optimization and in vitro characterization. *Nanomaterials*. 2016;6(6). doi:10.3390/nano6060116
45. Hoogenboezem EN, Duvall CL. Harnessing albumin as a carrier for cancer therapies. *Adv Drug Deliv Rev*. 2018;130:73–89. doi:10.1016/j.addr.2018.07.011
46. Li Y, Dai C, Hua Z, et al. A human serum albumin-indocyanine green complex offers improved tumor identification in fluorescence-guided surgery. *Transl Cancer Res*. 2024;13(1):437–452. doi:10.21037/tcr-23-2338
47. Sugio S, Kashima A, Mochizuki S, Noda M, Kobayashi K. Crystal structure of human serum albumin at 2.5 Å resolution. *Protein Eng Des Sel*. 1999;12(6):439–446. doi:10.1093/protein/12.6.439
48. Landsman ML, Kwant G, Mook GA, Zijlstra WG. Light-absorbing properties, stability, and spectral stabilization of indocyanine green. *J Appl Physiol*. 1976;40(4):575–583. doi:10.1152/jappl.1976.40.4.575
49. Bunschoten A, Buckle T, Kuil J, et al. Targeted non-covalent self-assembled nanoparticles based on human serum albumin. *Biomaterials*. 2012;33(3):867–875. doi:10.1016/j.biomaterials.2011.10.005
50. Yang X, Wang Y, Chen S, Zhang S, Cui C. Cetuximab-modified human serum albumin nanoparticles co-loaded with doxorubicin and mdr1 siRNA for the treatment of drug-resistant breast tumors. *Int J Nanomed*. 2021;16:7051–7069. doi:10.2147/IJN.S332830
51. Son S, Song S, Lee SJ, et al. Self-crosslinked human serum albumin nanocarriers for systemic delivery of polymerized siRNA to tumors. *Biomaterials*. 2013;34(37):9475–9485. doi:10.1016/j.biomaterials.2013.08.085
52. Meng R, Zhu H, Wang Z, Hao S, Wang B. Preparation of Drug-loaded albumin nanoparticles and its application in cancer therapy. *J Nanomater*. 2022;2022. doi:10.1155/2022/3052175.
53. Galiyeva A, Daribay A, Zhumagaliyeva T, Zhaparova L, Sadyrbekov D, Tazhbayev Y. Human serum albumin nanoparticles: synthesis, optimization and immobilization with antituberculosis drugs. *Polymers*. 2023;15(13). doi:10.3390/polym15132774
54. Maurisse R, De Semir D, Emamekhoo H, et al. Comparative Transfection of DNA into Primary and Transformed Mammalian Cells from Different Lineages; 2010. Available from: http://www.biomedcentral.com/1472-6750/10/9. Accessed April 3, 2025.
55. Zhong YQ, Wei J, Fu YR, et al. Toxicity of cationic liposome Lipofectamine 2000 in human pancreatic cancer Capan-2 cells. *Nan Fang Yi Ke da Xue Xue Bao*. 2008;28(11):1981–1984. PMID: 19033108
56. Kumar S, Stokes J, Singh UP, et al. Targeting Hsp70: a possible therapy for cancer. *Cancer Lett*. 2016;374(1):156–166. doi:10.1016/j.canlet.2016.01.056
57. Frisch K, Keiding S. Use of indocyanine green (ICG) in hepatology adv res gastroentero hepatol. *Adv Res Gastroentero Hepatol*. 2020;16(2). doi:10.19080/ARGH.2020.16.5559232
58. Imamura H, Sano K, Sugawara Y, Kokudo N, Makuuchi M. Assessment of hepatic reserve for indication of hepatic resection: decision tree incorporating indocyanine green test. *J Hepatobiliary Pancreat Surg*. 2005;12(1):16–22. doi:10.1007/s00534-004-0965-9
59. Yaseen MA, Yu J, Jung B, Wong MS, Anvari B. Biodistribution of encapsulated indocyanine green in healthy mice. *Mol Pharmaceut*. 2009;6:1321–1332. doi:10.1021/mp800270t
60. Chen S, Yu G, Zhang B, Wang Y, Zhang N, Chen Y. Human serum albumin (HSA) coated liposomal indocyanine green for in vivo tumor imaging. *RSC Adv*. 2016;6(18):15220–15225. doi:10.1039/C5RA25129J
61. Németh Z, Csóka I, Semnani Jazani R, et al. Quality by design-driven zeta potential optimisation study of liposomes with charge imparting membrane additives. *Pharmaceutics*. 2022;14(9). doi:10.3390/pharmaceutics14091798
62. Honary S, Zahir F. Effect of zeta potential on the properties of nano-drug delivery systems - A review (Part 2). *Trop J Pharm Res*. 2013;12(2):265–273. doi:10.4314/tjpr.v12i2.20
63. Behzadi S, Serpooshan V, Tao W, et al. Cellular uptake of nanoparticles: journey inside the cell. *Chem Soc Rev*. 2017;46(14):4218–4244. doi:10.1039/c6cs00636a
64. Li C, Zhang D, Pan Y, Chen B. Human serum albumin based nanodrug delivery systems: recent advances and future perspective. *Polymers*. 2023;15(16). doi:10.3390/polym15163354
65. Ji Q, Zhu H, Qin Y, et al. GP60 and SPARC as albumin receptors: key targeted sites for the delivery of antitumor drugs. *Front Pharmacol*. 2024:15. doi:10.3389/fphar.2024.1329636.
66. Rabbani G, Ahn SN. Structure, enzymatic activities, glycation and therapeutic potential of human serum albumin: a natural cargo. *Int J Biol Macromol*. 2019;123:979–990. doi:10.1016/j.ijbiomac.2018.11.053
67. Li R, Tsc N, Wang SJ, et al. Therapeutically reprogrammed nutrient signalling enhances nanoparticulate albumin bound drug uptake and efficacy in KRAS-mutant cancer. *Nat Nanotechnol*. 2021;16(7):830–839. doi:10.1038/s41565-021-00897-1
68. Zhou R, Zhang M, Xi J, et al. Gold nanorods-based photothermal therapy: interactions between biostructure, nanomaterial, and near-infrared irradiation. *Nanoscale Res Lett*. 2022;17(1). doi:10.1186/s11671-022-03706-3
69. He X, Li X, Tian W, et al. The role of redox-mediated lysosomal dysfunction and therapeutic strategies. *Biomed Pharmacother*. 2023:165. doi:10.1016/j.biopha.2023.115121.
70. Yu Z, Li W, Brunk UT. 3-Aminopropanal is a lysosomotropic aldehyde that causes oxidative stress and apoptosis by rupturing lysosomes. *APMIS*. 2003;111(6):643–652. doi:10.1034/j.1600-0463.2003.1110607.x
71. Li C, Tu L, Xu Y, et al. A NIR-Light-activated and lysosomal-targeted Pt(II) metallacycle for highly potent evoking of immunogenic cell death that potentiates cancer immunotherapy of deep-seated tumors. *Angew Chem Int Ed*. 2024;63(37). doi:10.1002/anie.202406392

72. Domagala A, Fidyt K, Bobrowicz M, Stachura J, Szczygiel K, Firczuk M. Typical and atypical inducers of lysosomal cell death: a promising anticancer strategy. *Int J mol Sci*. 2018;19(8). doi:10.3390/ijms19082256
73. Qu N, Song K, Ji Y, et al. Albumin nanoparticle-based drug delivery systems. *Int J Nanomed*. 2024;19:6945–6980. doi:10.2147/IJN.S467876
74. Zeeshan F, Madheswaran T, Panneerselvam J, Taliyan R, Kesharwani P. Human serum albumin as multifunctional nanocarrier for cancer therapy. *J Pharm Sci*. 2021;110(9):3111–3117. doi:10.1016/j.xphs.2021.05.001
75. Aloss K, Hamar P. Augmentation of the EPR effect by mild hyperthermia to improve nanoparticle delivery to the tumor. *Biochimica Et Biophysica Acta (BBA) – Rev Cancer*. 2024;1879(4):189109. doi:10.1016/J.BBCAN.2024.189109
76. ul HF, Nawaz A, Rehman MS, Ali MA, Dilshad SMR, Yang C. Prospects of HSP70 as a genetic marker for thermo-tolerance and immuno-modulation in animals under climate change scenario. *Animal Nutrition*. 2019;5(4):340–350. doi:10.1016/j.aninu.2019.06.005
77. Kim J, Kim J, Jeong C, Kim WJ. Synergistic nanomedicine by combined gene and photothermal therapy. *Adv Drug Deliv Rev*. 2016;98:99–112. doi:10.1016/j.addr.2015.12.018
78. Gentzler RD, Patel JD. Maintenance treatment after induction therapy in non-small cell lung cancer: latest evidence and clinical implications. *Ther Adv Med Oncol*. 2014;6(1):4–15. doi:10.1177/1758834013510589